FULL PAPER

Dalton
www.rsc.org/dalton

Embracing ligands. Synthesis, characterisation and the correlation between ^{59}Co NMR and ligand field parameters of Co(III) complexes with a new class of nitrogen–thioether multidentate ligand †

Clint A. Sharrad,[a] Germán E. Cavigliasso,[b] Robert Stranger[b] and Lawrence R. Gahan*[a]

[a] *Chemistry Department, The University of Queensland, Brisbane, QLD 4072, Australia*

[b] *Department of Chemistry, Faculty of Science, Australian National University, ACT 0200 Australia*

Received 20th October 2003, Accepted 22nd December 2003
First published as an Advance Article on the web 3rd February 2004

The syntheses of the hexadentate ligands 2,2,10,10-tetra(methyleneamine)-4,8-dithiaundecane (PrN_4S_2amp), 2,2,11,11-tetra(methyleneamine)-4,9-dithiadodecane (BuN_4S_2amp), and 1,2-bis(4,4-methyleneamine)-2-thiapentyl)benzene (XyN_4S_2amp) are reported and the complexes $[Co(RN_4S_2amp)]^{3+}$ (R = Pr, Bu, Xy) characterised by single crystal X-ray study. The low-temperature (11 K) absorption spectra have been measured in Nafion films. From the observed positions of both spin-allowed $^1A_{1g} \longrightarrow {}^1T_{1g}$ and $^1A_{1g} \longrightarrow {}^1T_{2g}$ and spin forbidden $^1A_{1g} \longrightarrow {}^3T_{1g}$ and $^1A_{1g} \longrightarrow {}^3T_{2g}$ bands, octahedral ligand-field parameters ($10D_q$, B and C) have been determined. DFT calculations suggest that significant interaction between the d–d and CT excitations occurs for the complexes. The calculations offer an explanation for the observed deviations from linearity of the relationship between ^{59}Co magnetogyric ratio and $\beta(\Delta E)^{-1}$ (β = the nephelauxetic ratio; ΔE the energy of the $^1A_{1g} \longrightarrow {}^1T_{1g}$ transition) for a series of amine and mixed amine/thioether donor complexes.

Introduction

We have investigated the further development of a hexadentate ligand topology in which bifurcations of the chain occur at atoms other than donor atoms.[1–3] These ligands, known as *amplectors*,[3] develop previously established themes in the coordination chemistry of thioether/nitrogen ligands. Our interest previously has been in the synthesis, electron transfer properties, and visible spectroscopy of complexes of nickel(II), copper(II) and cobalt(III).[3–8] More recently our interest has turned to the ^{59}Co NMR of these systems, particularly the relationship between the magnetogyric ratio for ^{59}Co (γ_{Co}) and the energy of the $^1A_{1g} \longrightarrow {}^1T_{1g}$ transition.

It has been proposed that a linear correlation between the magnetogyric ratio (γ_{Co}) and $E(^1A_{1g} \longrightarrow {}^1T_{1g})^{-1}$, $(\Delta E)^{-1}$, would be expected for a series of complexes in which d orbitals are affected by ligators in a similar way.[9–16] To allow for effects such as the extent of covalent bonding to be included into the correlation, the nephelauxetic ratio, β (= B/B_o), was incorporated. Thus, for a series of octahedral cobalt(III) complexes with both first- and second-row ligators {O_6, N_6, C_6, S_6, P_6 and Se_6} a linear correlation between the ^{59}Co magnetogyric ratio and $\beta(\Delta E)^{-1}$ was observed.[14] The common intercept, $\gamma_0(^{59}Co)$, was found to be 10.06 ± 0.01 MHz T^{-1}. Juranić also included structural correction factors to account for deviations from linearity.[16]

Bramley *et al.* investigated a series of orthoaxial and non-orthoaxial cobalt(III) complexes.[15] The orthoaxial examples included homoleptic complexes, like $[Co(H_2O)_6]^{3+}$ and $[Co(NH_3)_6]^{3+}$, and mixed donor complexes, like $[Co(NH_3)_5(CN)]^{2+}$ and $[Co(NH_3)_5F]^{2+}$. These authors incorporated an intermediate cubic-field approach and included first-order low-symmetry corrections to the cubic field. The Racah parameter B and subsequently β (= B/B_o) were included in the analysis. For the orthoaxial complexes $\gamma_0(^{59}Co)$ was determined to be 10.048 ± 0.003 MHz T^{-1}, in excellent agreement with values found previously.[15] For nonorthoaxial complexes, for example tris-bidentate complexes like $[Co(en)_3]^{3+}$ and $[Co(ox)_3]^{3-}$ where the chelated donor atoms deviate slightly from positions of octahedral geometry, Bramley *et al.* concluded that the situation was not so simple. In this case the energies of the maxima for the first and second cubic parentage bands did not represent the average cubic energies very well. In their analysis Bramley *et al.* used three ligand field parameters (the cubic parameter, Δ, and two low-symmetry parameters, $B_{Schäffer}$ and D)[17] which describe trigonal complexes.[15] For the nonorthoaxial complexes Bramley found that a plot of γ_{Co} *versus* $\beta(\Delta E)^{-1}$ was linear with $\gamma_0(^{59}Co)$ = 10.04 ± 0.05 MHz T^{-1}. However, exclusion from the analysis of two complexes with sulfur donor ligands (a xanthate and a dithiophosphate) altered the intercept appreciably ($\gamma_0(^{59}Co)$ = 9.85 ± 0.04 MHz T^{-1}). Bramley concluded that the relationship was not well understood for nonorthoaxial systems.[15]

The series of complexes $[Co(RN_4S_2amp)]^{3+}$ reported in a previous paper (R = Et)[3] and in this work (R = Pr, Bu, Xy) (Chart 1), in combination with cobalt(III) complexes of homoleptic N_6[18–21] and heteroleptic ($N_{6-x}S_x$; x = 1, 2, 3) ligands reported previously[3–8] offer an opportunity to explore further the relationship between ^{59}Co NMR shifts and the energies of the $^1A_{1g} \longrightarrow {}^1T_{1g}$ transition.

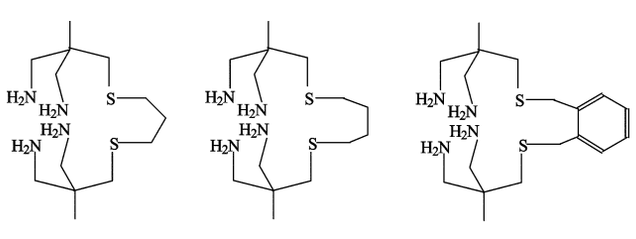

Chart 1

Results and discussion

Nomenclature

The nomenclature employed to describe these amplector (amp) ligands has been described in a previous publication.[3] Thus for PrN_4S_2amp, the prefix Pr denotes the propyl hinge and N_4S_2

† Electronic supplementary information (ESI) available: Nafion film UV-visible absorption spectra of $[Co(PrN_4S_2amp)]^{3+}$ at room temperature and 14 K. See http://www.rsc.org/suppdata/dt/b3/b313189k/

DOI: 10.1039/b313189k

Table 1 Crystal data

	$[Co(PrN_4S_2amp)]Cl(ClO_4)_2\cdot 2H_2O$	$[Co(BuN_4S_2amp)]Cl_2(ClO_4)\cdot 2H_2O$	$[Co(XyN_4S_2amp)]Br_3\cdot 3H_2O$
Empirical formula	$C_{13}H_{36}Cl_3CoN_4O_{10}S_2$	$C_{14}H_{38}Cl_3CoN_4O_6S_2$	$C_{36}H_{80}Br_6Co_2N_8O_6S_4$
M	637.86	587.88	1446.64
Crystal system	Monoclinic	Monoclinic	Monoclinic
Space group	$P2_1/n$	$P2_1/n$	$P2_1/n$
a/Å	10.334(1)	10.873(1)	23.719(5)
b/Å	15.389(2)	18.484(1)	9.7912(9)
c/Å	16.216(3)	13.636(2)	24.073(2)
β/°	99.81(1)	112.311(9)	99.626(7)
V/Å^3	2541.1(6)	2535.4(5)	5511.9(13)
Z	4	4	4
μ/cm^{-1}	12.09	11.94	51.50
T/K	293(2)	293(2)	293(2)
$R(F_o)$	0.0596	0.0542	0.0591
R_w	0.0702	0.0667	0.1702

refers to the tetraamine-dithioether donor set of the ligand. Similar nomenclature applies to the BuN_4S_2amp and XyN_4S_2amp systems.

Synthesis

The synthetic procedure follows that described previously for the ligand EtN_4S_2amp.[3] Replacing 1,2-ethanedithiol in that synthesis with 1,3-propanedithiol, 1,4-butanedithiol, and 1,2-xylenedithiol in the present synthetic procedures and subsequent complexation of the resulting ligands resulted in the isolation of $[Co(RN_4S_2amp)]^{3+}$ (R = Pr, Bu, Xy).[3] The $[Co(XyN_4S_2amp)]^{3+}$ complex was found to be stable in acidic solution but decomposed to several products over a period of days in aqueous solution at pH 7.

NMR spectra

The ^{13}C NMR spectrum of $[Co(PrN_4S_2amp)]^{3+}$ displayed the expected seven-line spectrum with the resonances of the methylene carbons adjacent to the thioether donors (δ_C −32.3, −29.0 ppm) and the central methylene carbon of the dithiol hinge (δ_C −44.8 ppm) shifted up field from those observed in the ethyl analogue. The spectrum for $[Co(BuN_4S_2amp)]^{3+}$ also exhibited a seven-line spectrum where the resonances for the methylene carbons adjacent to the thioethers are shifted markedly downfield (δ_C −22.4, −21.0 ppm) in comparison to the Co(III) complexes of EtN_4S_2amp and PrN_4S_2amp. The resonance of the two central carbon atoms of the dithio-hinge was found at δ_C −37.7 ppm. The spectrum of $[Co(XyN_4S_2amp)]^{3+}$ exhibited nine resonances, with those for the methylene carbons adjacent to the thioethers again shifted upfield (δ_C −30.3, −29.0 ppm) compared to those of $[Co(EtN_4S_2amp)]^{3+}$.[3]

Structures

The structures of the complex cations $[Co(PrN_4S_2amp)]^{3+}$, $[Co(BuN_4S_2amp)]^{3+}$ and $[Co(XyN_4S_2amp)]^{3+}$ (crystal data, Table 1) show the coordination of the four primary amine and two thioether donors to the metal ion in each case. For $[Co(PrN_4S_2amp)]Cl(ClO_4)_2\cdot 2H_2O$ (Fig. 1), and $[Co(BuN_4S_2amp)]Cl_2(ClO_4)\cdot 2H_2O$ (Fig. 2) the structures consist of the complex cation, each having the *lel* conformation,[22] and associated mixed anions. The structure of $[Co(XyN_4S_2amp)]Br_3\cdot 3H_2O$ (Fig. 3) consists of two crystallographically independent molecular cations, six bromide anions and six water molecules within the asymmetric unit. $[Co(XyN_4S_2amp)]Br_3\cdot 3H_2O$ adopts the *ob* conformation[22] with the vector between C6 and C13 (or C24 and C31) oblique to the pseudo-C_3 axis. However, unlike *ob* conformations with five membered chelate rings, the *ob* conformation for the XyN_4S_2amp was attained with both coordinated thioethers adopting the same chirality. The *ob* conformation is dictated by the strained nature of the seven membered chelate ring and the aromatic moiety reducing the flexibility of the ring. There are no significant differences between the structures of the molecular cations in the asymmetric unit. All of the six-membered chelate rings have the unsymmetrical skew boat conformation.

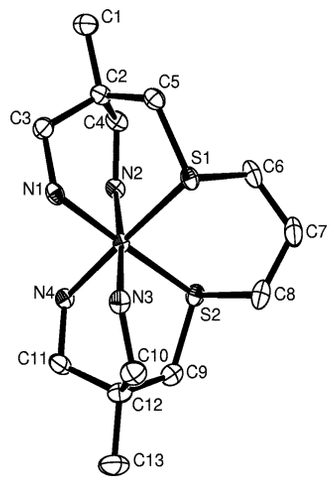

Fig. 1 ORTEP plot of the complex cation of $[Co(PrN_4S_2amp)]Cl(ClO_4)_2\cdot 2H_2O$, with crystallographic numbering. Probability ellipsoids of 30% are shown.

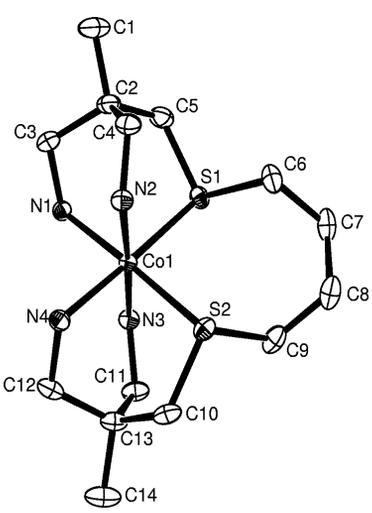

Fig. 2 ORTEP plot of the complex cation of $[Co(BuN_4S_2amp)]Cl_2(ClO_4)\cdot 2H_2O$, with crystallographic numbering. Probability ellipsoids of 30% are shown.

The Co–N bond lengths for $[Co(PrN_4S_2amp)]^{3+}$ (average 1.981(6) Å), and $[Co(BuN_4S_2amp)]^{3+}$ (average 1.981(2) Å) (Tables 2 and 3) are similar to those reported for the hexadentate complex $[Co(N_4S_2)]^{3+}$ (average 1.983(5) Å) (N_4S_2 = 5-(4-amino-2-azabutyl)-5-methyl-3,7-dithianonane-1,9-diamine)[7]

Table 2 Selected interatomic distances (Å) and angles (°) for $[Co(PrN_4S_2amp)]Cl(ClO_4)_2\cdot 2H_2O$

Co(1)–N(1)	1.979(4)	Co(1)–N(2)	1.990(4)
Co(1)–N(3)	1.982(4)	Co(1)–N(4)	1.974(4)
Co(1)–S(1)	2.2426(13)	Co(1)–S(2)	2.2608(14)
N(1)–Co(1)–N(2)	90.06(17)	N(3)–Co(1)–S(2)	93.03(13)
N(1)–Co(1)–N(3)	86.72(17)	N(4)–Co(1)–N(1)	93.69(17)
N(1)–Co(1)–S(1)	87.67(12)	N(4)–Co(1)–N(2)	87.51(16)
N(1)–Co(1)–S(2)	178.37(12)	N(4)–Co(1)–N(3)	89.36(17)
N(2)–Co(1)–S(1)	92.77(12)	N(4)–Co(1)–S(1)	178.61(13)
N(2)–Co(1)–S(2)	90.28(13)	N(4)–Co(1)–S(2)	87.91(12)
N(3)–Co(1)–N(2)	175.35(18)	S(1)–Co(1)–S(2)	90.73(5)
N(3)–Co(1)–S(1)	90.44(13)		

Table 3 Selected interatomic distances (Å) and angles (°) for $[Co(BuN_4S_2amp)]Cl_2(ClO_4)\cdot 2H_2O$

Co(1)–N(1)	1.982(3)	Co(1)–N(2)	1.978(3)
Co(1)–N(3)	1.983(3)	Co(1)–N(4)	1.980(3)
Co(1)–S(1)	2.2552(11)	Co(1)–S(2)	2.2636(12)
N(1)–Co(1)–N(3)	87.20(14)	N(3)–Co(1)–S(1)	89.42(10)
N(1)–Co(1)–S(1)	87.24(10)	N(3)–Co(1)–S(2)	91.24(10)
N(1)–Co(1)–S(2)	177.62(10)	N(4)–Co(1)–N(1)	90.63(14)
N(2)–Co(1)–N(1)	90.19(14)	N(4)–Co(1)–N(3)	90.84(14)
N(2)–Co(1)–N(3)	177.06(14)	N(4)–Co(1)–S(1)	177.84(11)
N(2)–Co(1)–N(4)	87.83(14)	N(4)–Co(1)–S(2)	87.59(10)
N(2)–Co(1)–S(1)	91.82(10)	S(1)–Co(1)–S(2)	94.55(4)
N(2)–Co(1)–S(2)	91.33(10)		

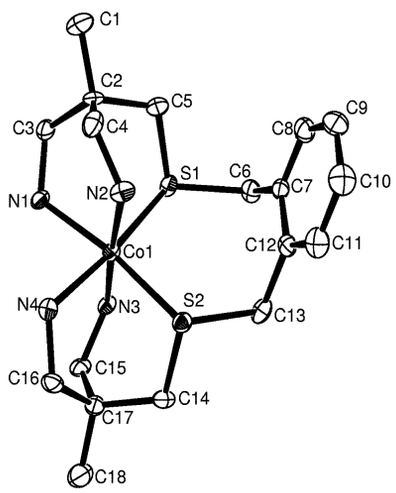

Fig. 3 ORTEP plot of a complex cation of $[Co(XyN_4S_2amp)]Br_3\cdot 3H_2O$, with crystallographic numbering. Probability ellipsoids of 30% are shown.

and $[Co(EtN_4S_2amp)]^{3+}$ (average 1.984(3) Å)[3] and appear typical of the normal range of Co–N bond lengths in hexaamine encapsulating ligands of cobalt(III).[23] For $[Co(XyN_4S_2amp)]^{3+}$ the Co–N bond lengths are variable (1.955(7) −2.017(8) Å; average 1.99(2) Å) (Table 4) with the majority found at the longer end of the range of observed Co(III)–amine bond lengths (1.94–2.01 Å).[23] The Co–S bond lengths for $[Co(PrN_4S_2amp)]^{3+}$ and $[Co(BuN_4S_2amp)]^{3+}$ (average 2.252(9) and 2.259(4) Å, respectively) are distinctly longer in comparison to $[Co(EtN_4S_2amp)]^{3+}$ (2.2159(13) Å)[3] showing an increase in Co–S bond length with increasing dithio-chelate ring size. The Co–S bond lengths for $[Co(XyN_4S_2amp)]^{3+}$ (average 2.267(6) Å) are slightly longer than those of $[Co(BuN_4S_2amp)]^{3+}$, both complexes having seven membered dithio-chelate rings. While the Co–S bond length for $[Co(EtN_4S_2amp)]^{3+}$ is found at the short end of the narrow range of cobalt(III)–thioether bond lengths for these types of complexes (2.194(5) −2.275(3) Å),[24–26] for $[Co(PrN_4S_2amp)]^{3+}$, $[Co(BuN_4S_2amp)]^{3+}$ and $[Co(XyN_4S_2amp)]^{3+}$ the Co–S bond lengths fall at the longer end of this range. There seems to be no general trend in Co(III)–S bond lengths from five to seven membered dithio-chelate rings for other ligand topologies.

Table 4 Selected interatomic distances (Å) and angles (°) for $[Co(XyN_4S_2amp)]Br_3\cdot 3H_2O$

Co(1)–N(1)	2.004(7)	Co(2)–N(5)	1.999(7)
Co(1)–N(2)	1.987(8)	Co(2)–N(6)	1.983(8)
Co(1)–N(3)	1.955(7)	Co(2)–N(7)	1.959(7)
Co(1)–N(4)	1.991(8)	Co(2)–N(8)	2.017(8)
Co(1)–S(1)	2.276(3)	Co(2)–S(3)	2.266(3)
Co(1)–S(2)	2.261(3)	Co(2)–S(4)	2.265(3)
N(1)–Co(1)–S(1)	85.7(2)	N(5)–Co(2)–N(8)	86.6(3)
N(1)–Co(1)–S(2)	169.8(2)	N(5)–Co(2)–S(3)	85.1(2)
N(2)–Co(1)–N(1)	89.8(3)	N(5)–Co(2)–S(4)	170.7(2)
N(2)–Co(1)–N(4)	93.3(3)	N(6)–Co(2)–N(5)	90.5(3)
N(2)–Co(1)–S(1)	89.4(3)	N(6)–Co(2)–N(8)	93.4(3)
N(2)–Co(1)–S(2)	88.7(2)	N(6)–Co(2)–S(3)	89.7(2)
N(3)–Co(1)–N(1)	92.0(3)	N(6)–Co(2)–S(4)	88.6(2)
N(3)–Co(1)–N(2)	175.8(4)	N(7)–Co(2)–N(5)	91.2(3)
N(3)–Co(1)–N(4)	90.6(3)	N(7)–Co(2)–N(6)	176.4(3)
N(3)–Co(1)–S(1)	87.0(2)	N(7)–Co(2)–N(8)	89.9(3)
N(3)–Co(1)–S(2)	90.1(2)	N(7)–Co(2)–S(3)	87.2(2)
N(4)–Co(1)–N(1)	86.7(3)	N(7)–Co(2)–S(4)	90.2(2)
N(4)–Co(1)–S(1)	172.0(2)	N(8)–Co(2)–S(3)	171.1(3)
N(4)–Co(1)–S(2)	83.3(2)	N(8)–Co(2)–S(4)	84.3(3)
S(2)–Co(1)–S(1)	104.34(10)	S(4)–Co(2)–S(3)	104.09(10)

The S–Co–S bite angle for $[Co(PrN_4S_2amp)]^{3+}$ (90.73(5)°) (Table 2) shows only a slight increase in comparison to that reported for $[Co(EtN_4S_2amp)]^{3+}$ (89.72(7)°). For $[Co(BuN_4S_2amp)]^{3+}$ and $[Co(XyN_4S_2amp)]^{3+}$ (Tables 3 and 4) complexes with seven membered dithio-chelate rings, there is a marked increase in this bite angle (94.55(4)° and average 104.2(1)°, respectively) reflecting the greater strain of the seven membered dithio-chelate ring. The C–C–C angles for the carbon atoms within the dithio-chelate ring for both $[Co(PrN_4S_2amp)]^{3+}$ and $[Co(BuN_4S_2amp)]^{3+}$ are all approximately 116°, considerably distorted from ideal tetrahedral geometry.

The larger dithio-hinges also result in a bending of the complex about the cobalt centre and force the apices of the ligand away from the pseudo-C_3 axis. This is clearly shown by comparing the ligand bend angles (defined as the angle of the complexes between the quaternary carbon, the cobalt centre and the opposite quaternary carbon) for $[Co(EtN_4S_2amp)]^{3+}$ (C2–Co1–C2#1, 174.2(1)°),[3] $[Co(PrN_4S_2amp)]^{3+}$ (C2–Co–C12, 171.3(2)°), $[Co(BuN_4S_2amp)]^{3+}$ (C2–Co–C13, 167.5(1)°) and $[Co(XyN_4S_2amp)]^{3+}$ (C2–Co1–C17: 166.6(3)°; C20–Co2–C35: 166.9(3)°). In comparison, the relatively strain free hexaamine complex $[Co(tame)_2]^{3+}$, which has the same apical moieties as the amplectors but with no hinge linkers, exhibits a bend angle of 178.9°.[27]

Geometry optimizations

The calculated Co–S and Co–N bond distances and S–Co–S and N–Co–N bond angles, obtained by three different computational approaches (denoted LDA/TZP, PBE/TZP and PBE/ZORA/TZ2P), are compared with experimental results in Table 5.

The experimental structures are reasonably well reproduced by the three approaches. In particular, all methods correctly predict the variations in the S–Co–S angle, the parameter that is most significantly affected by the changes in the R fragment (connecting the S sites). The N–Co–N angles are also closely reproduced, with only minor differences observed between the values predicted by each individual approach.

The computational results for the Co–S and Co–N bond lengths are somewhat more variable. The Co–N distances predicted by calculations using the local (LDA) functional compare remarkably well with the experimental values, but the agreement is not as satisfactory for the Co–S distances. These are better reproduced by the methods incorporating (PBE) gradient corrections, in particular when larger (TZ2P) basis sets

Table 5 Comparison of calculated and experimental structural parameters (distances in Å, angles in degrees) for $[Co(RN_4S_2amp)]^{3+}$ complexes

Complex	Parameter	LDA/TZP	PBE/TZP	PBE/ZORA/TZ2P	Experiment
$[Co(EtN_4S_2amp)]^{3+}$	Co–S	2.20	2.25	2.23-2.24	2.22
	Co–N	1.97–1.99	2.02–2.05	2.02–2.05	1.98–1.99
	S–Co–S	89.6	89.3	89.6	89.7
	N–Co–N (*cis*)	87.6–94.2	86.9–94.0	86.8–94.0	88.8–92.8
	N–Co–N (*trans*)	177.5	178.9	178.8	177.5
$[Co(PrN_4S_2amp)]^{3+}$	Co–S	2.21	2.28	2.25–2.26	2.24–2.26
	Co–N	1.97–1.99	2.03–2.06	2.02–2.05	1.98–1.99
	S–Co–S	91.8	91.6	91.8	90.7
	N–Co–N (*cis*)	87.9–94.6	88.4–95.2	88.2–94.9	86.7–93.7
	N–Co–N (*trans*)	177.5	177.6	176.9	175.4
$[Co(BuN_4S_2amp)]^{3+}$	Co–S	2.22	2.30	2.28	2.26
	Co–N	1.96–1.99	2.02–2.05	2.01–2.05	1.98
	S–Co–S	93.7	93.7	94.0	94.6
	N–Co–N (*cis*)	88.4–92.0	88.2–93.2	88.9–92.6	87.2–90.8
	N–Co–N (*trans*)	177.3	177.0	177.0	177.1
$[Co(XyN_4S_2amp)]^{3+}$	Co–S	2.21–2.22	2.29	2.27	2.26–2.28
	Co–N	1.96–2.01	2.01–2.08	2.00–2.08	1.96–2.02
	S–Co–S	104.0	102.7	102.8	104.1–104.3
	N–Co–N (*cis*)	85.6–95.8	87.8–95.0	87.2–95.0	86.6–93.4
	N–Co–N (*trans*)	174.9	176.1	176.3	175.8–176.4

and (ZORA) relativistic corrections are introduced. However, the Co–N distances predicted by the PBE calculations are relatively longer than those observed experimentally or obtained from LDA calculations.

In general, both the LDA/TZP and the PBE/ZORA/TZ2P methods can be considered to be satisfactory approaches for the computational prediction of the geometrical parameters of $[CoRN_4S_2amp]^{3+}$ complexes.

Redox behaviour

The redox potentials of the complexes were determined by cyclic voltammetry in aqueous solution (0.1 M $NaClO_4$) at various pH values with glassy carbon, platinum and hanging mercury drop working electrodes (Ag/AgCl/KCl reference electrode). Metal-based irreversible redox processes were observed for each complex under all conditions employed. The cathodic peak attributed to the $Co^{3+/2+}$ couple shifts to less negative potentials as the size of the dithio-chelate ring increases ($[Co(RN_4S_2amp)]^{3+/2+}$,(R = Et, −330 mV; Pr, −301 mV; Bu, −201 mV; Xy, −40 mV: 0.1 M $NaClO_4$, pH <5). Increasing the size of the coordination sphere by increasing the size of the dithio-chelate ring allows for easier reduction of the Co(III) complex. The cathodic peak potentials observed for $[Co(EtN_4S_2amp)]^{3+/2+}$ and $[Co(PrN_4S_2amp)]^{3+/2+}$ are comparable with those observed for $[Co(N_4S_2)]^{3+}$ (-349 mV: 0.1 M $NaClO_4$).[3,6]

UV-visible spectroscopy

The room temperature solution UV-visible spectra of $[Co(PrN_4S_2amp)]^{3+}$, $[Co(BuN_4S_2amp)]^{3+}$ and $[Co(XyN_4S_2amp)]Br_3$ were recorded in aqueous solution. In each case the peak attributed to the $^1A_{1g} \longrightarrow {}^1T_{1g}$ transition is clearly seen. The higher energy $^1A_{1g} \longrightarrow {}^1T_{2g}$ transition is seen as subtle shoulder and as a distinct shoulder on an intense charge transfer band for $[Co(PrN_4S_2amp)]^{3+}$ and $[Co(BuN_4S_2amp)]^{3+}$, respectively, while for $[Co(XyN_4S_2amp)]^{3+}$ the transition is totally obscured by the intense charge transfer band. No spin forbidden transitions were observed at room temperature in aqueous solution. Data for these complexes as well as a range of other N_6 and $N_{6-x}S_x$ (x = 1, 2, 3) complexes are collected in Table 6.

The absorption spectra were also recorded in a Nafion film at 273 and 14 K. The higher energy $^1A_{1g} \longrightarrow {}^1T_{2g}$ absorption for $[Co(PrN_4S_2amp)]^{3+}$ becomes more pronounced at low temperatures (Electronic Supplementary Information †). To locate the spin forbidden bands $^1A_{1g} \longrightarrow {}^3T_{1g}$ and $^1A_{1g} \longrightarrow {}^3T_{2g}$ at 14 K highly concentrated solutions and stacked Nafion films were required with both transitions observed for $[Co(PrN_4S_2amp)]^{3+}$ (13400, 17100 cm^{-1}). For $[Co(BuN_4S_2amp)]^{3+}$ the $^1A_{1g} \longrightarrow {}^1T_{2g}$ transition is seen as a distinct shoulder (26670 cm^{-1}) at low temperature while the $^1A_{1g} \longrightarrow {}^3T_{2g}$ transition (17100 cm^{-1}) is the only spin forbidden band observed. The Nafion spectra of $[Co(XyN_4S_2amp)]^{3+}$ shows that the $^1A_{1g} \longrightarrow {}^1T_{2g}$ band is completely obscured by a charge transfer band and cannot be resolved even at low temperature (14 K), while the spin forbidden transition to the $^3T_{2g}$ state (17240 cm^{-1}) is seen at 14 K.

In situations where the spin allowed and spin forbidden transitions are observed or determined using a peak fitting procedure, and assuming O_h symmetry, the following perturbation expressions corrected for configuration interaction can be used to uniquely determine the spectroscopic parameters $10D_q$, B and C:[7,28–30]

$$\begin{aligned}
E(^1A_{1g} \longrightarrow {}^1T_{1g}) &= 10D_q - C + (5BC + 7B^2 + C^2)/5D_q \\
E(^1A_{1g} \longrightarrow {}^1T_{2g}) &= 10D_q - C + 16B + (3BC - 27B^2 + C^2)/5D_q \\
E(^1A_{1g} \longrightarrow {}^3T_{1g}) &= 10D_q - 3C + (5BC - 11B^2 + C^2)/5D_q \\
E(^1A_{1g} \longrightarrow {}^3T_{2g}) &= 10D_q - 3C + 8B + (3BC - 21B^2 + C^2)/5D_q
\end{aligned} \quad (1)$$

Using this approach the best fit parameters for $10D_q$, B and C were obtained from the determined band positions in the low temperature spectra for the $[Co(PrN_4S_2amp)]^{3+}$ (B = 437 cm^{-1}, C = 3190 cm^{-1} and $10D_q$ = 21930 cm^{-1}). The C/B ratio for this complex is 7.3:1 which is one of the largest such values observed for a Co(III) complex.[4,7,8,24,29] For $[Co(BuN_4S_2amp)]^{3+}$, using the same approach, $10D_q$ = 21780 cm^{-1} with B = 450 cm^{-1} and C = 3040 cm^{-1} (C/B = 6.8). Difficulties associated with the unequivocal assignment of the energy of the $^1A_{1g} \longrightarrow {}^3T_{2g}$ spin forbidden band and the inability to observe the $^1A_{1g} \longrightarrow {}^1T_{2g}$ spin allowed band for the $[Co(XyN_4S_2amp)]^{3+}$ complex, precluded a complete analysis of the data. However, assuming $C = 6B$ for this complex, the value of B for $[Co(XyN_4S_2amp)]^{3+}$ at 467 cm^{-1} is similar to those of $[Co(PrN_4S_2amp)]^{3+}$ and $[Co(BuN_4S_2amp)]^{3+}$.

The magnitude of $10D_q$ for the $[Co(RN_4S_2amp)]^{3+}$ (R = Pr, Bu, Xy) complexes is similar to most Co(III) complexes with mixed donor nitrogen–thioether ligands.[4,7,8,24] However, the value of B appears to be around 100 cm^{-1} lower than that for $[Co(EtN_4S_2amp)]^{3+}$ (B = 551 cm^{-1}) and lower than that for the $[Co(N_4S_2)]^{3+}$ and $[Co(AMN_4S_2sarH)]^{4+}$ complexes (516 $cm^{-1}$and 526 cm^{-1}, respectively).

Table 6 Spectroscopic parameters for Co(III) complexes of nitrogen–thioether ligands[a]

Ligand[b]	Donor set	$^1A_{1g} \longrightarrow {}^1T_{1g}$/cm^{-1}	$^1A_{1g} \longrightarrow {}^1T_{2g}$/cm^{-1}	$^1A_{1g} \longrightarrow {}^3T_{1g}$/cm^{-1}	$^1A_{1g} \longrightarrow {}^3T_{2g}$/cm^{-1}	$10D_q$/cm^{-1}	B/cm^{-1}	C[d]/cm^{-1}	$\beta(\Delta E)^{-1}$[e]/nm	γ_{Co}[f]/MHz T^{-1}	Compound no.[g]	Ref.
N_3S_3	3N 3S	20860	27280	14535	17625	23360	452	3040	203.5	10.1507	1	4[i]
CLN_3S_3sar	3N 3S	20500	27100	—	—	21800	475	—	217.6	10.1503	2	[j]
$AMN_3S_3sarH^+$	3N 3S	20460	26960	14145	17240	21920	459	3030	210.6	10.1506	3	4[i]
N_4S_2	4N 2S	20800	27950	—	—	22140	516	—	232.9	10.1602	4	6[j]
$AMN_4S_2sarH^+$	4N 2S	20450	27700	—	—	21750	526	—	241.5	10.1604	5	6[j]
EtN_4S_2amp	4N 2S	21140	28800	13800	17400	22570	551	3500	244.7	10.1627	6	3[i]
$(daes)_2$	4N 2S	20600	28100	—	—	21900	549	—	250.2	10.1618	7	49[j]
N_5S	5N S	20900	28700	—	—	22200	572	—	257.0	10.1686	8	8[j]
$AZAN_5Ssar$	5N S	20700	28200	—	—	22000	547	—	248.1	10.1686	9	[j]
HN_5Ssar	5N S	20700	28300	—	—	22000	551	—	249.9	10.1686	10	[j]
CLN_5Ssar	5N S	20600	28300	—	—	21900	565	—	257.5	10.1688	11	[j]
$(en)_3$	6 N	21500	29600	13700	17500	23000	583	3730	254.6	10.178	12	50
sep	6 N	21200	29400	—	—	22400	607	—	268.8	10.1758	13	51[j]
$diAMN_6sarH_2^{2+}$	6 N	21100	29030	—	—	22400	583	—	259.4	10.1752	14	18[j]
$(NH_3)_6$	6 N	21200	29550	13000	17200	22400	621	3790	275.0	10.1881	15	50
$diNON_6sar$	6 N	21120	29110	—	—	22390	588	—	261.4	10.1752	16	23[j]
AMN_6sarH^+	6 N	21200	29000	—	—	22500	571	—	252.9	10.1748	17	18[j]
sen	6 N	21400	29400	—	—	22710	587	—	257.6	10.1756	18	52[j]
PrN_4S_2amp	4N 2S	20590	26400[c]	13400	17100	21930	437	3190	199.3	10.1676	19	[i]
									244.9		19a[h]	
BuN_4S_2amp	4N 2S	20350	26670	—	17100	21780	450	3040	207.6	10.1686	20	[i]
									253.8		20a[h]	
XyN_4S_2amp	4N 2S	19890	—	—	17200	21200	467	—	220.5	10.1711	21	[i]
									267.7		21a[h]	

[a] Parameters obtained the best fit of all presented energies to eqn. (1). All energies determined by Peakfit[48] using the residuals method with Gaussian + Lorentzian amplitude curves with no base line unless otherwise stated. [b] Ligand nomenclature described below Table 7. [c] Peak fitted by Peakfit[48] using the residuals method with Gaussian amplitude curve and linear baseline. [d] For values of C not given, $C = 6\,B$ is assumed in order to determine $10D_q$ and B. [e] $\beta = B/B_0$ ($B_0 = 1065$ cm^{-1}).[30] [f] $\gamma_{Co} = \gamma_s(1+\delta_{Co})$ where $\gamma_s = 10.1057$ MHz T^{-1} (the magnetogyric ratio of $[Co(CN)_6]^{3-}$); δ_{Co} is given in Table 7. [g] see Fig. 5. [h] See text for details. [i] Spectra obtained from Nafion films at ≤ 14 K. [j] Solution spectra.

Table 7 ^{59}Co NMR data[a]

Ligand [b]	Donor set	Anion	δ_{Co} (ppm)	$\nu_{1/2}$/Hz[d]
N_3S_3	3N 3S	$(ClO_4)_3$	4455	510
CLN_3S_3sar	3N 3S	$(ClO_4)_3$	4413	2100
$AMN_3S_3sarH^+$	3N 3S	Cl_4	4448	2700
N_4S_2	4N 2S	$(ClO_4)_3$	5390	900
$AMN_4S_2sarH^+$	4N 2S	$(ClO_4)_4$	5416	4000
EtN_4S_2amp	4N 2S	$Cl(ClO_4)_2$	5638	740
$(daes)_2$	4N 2S	Br_3	5553	230
N_5S	5N S	$(ClO_4)_3$	6229	900
$AZAN_5Ssar$	5N S	$(ClO_4)_3$	6229	1000
HN_5Ssar	5N S	$(ClO_4)_3$	6224	1800
CLN_5Ssar	5N S	$(ClO_4)_3$	6250	1400
$(en)_3$	6 N	Cl_3	7125[c]	100
sep	6 N	Cl_3	6941	260
$diAMN_6sarH_2^{2+}$	6 N	Cl_5	6877	1400
$(NH_3)_6$	6 N	Cl_3	8152	160
diNOsar	6 N	Cl_3	6875	1200
AMN_6sarH^+	6 N	Cl_4	6839	840
sen	6 N	$(ClO_4)_3$	6920	250
PrN_4S_2amp	4N 2S	$Cl(ClO_4)_2$	6125	1700
BuN_4S_2amp	4N 2S	$Cl_2(ClO_4)$	6223	2700
XyN_4S_2amp	4N 2S	Br_3	6476	12000

[a] All samples were recorded in H_2O at a concentration of 0.1 M. Chemical shifts (ppm) are primarily referenced to $[Co(en)_3]Cl_3$ at 7125 ppm with $K_3[Co(CN)_6]$ used as a secondary reference (δ_{Co} 0 ppm). Temp. = 301 K. Absolute error of ± 50 ppm. Relative error of ± 2 ppm when $\nu_{1/2} \leq 500$ Hz, ≤ 5 ppm when 500 Hz ≤ $\nu_{1/2}$ ≤ 1000 Hz, ± 10 ppm when 1000 ≤ $\nu_{1/2}$ ≤ 2000 Hz, ± 25 ppm when 1000 ≥ $\nu_{1/2}$ ≤ 2000 Hz, ± 25 ppm when 2000 ≤ $\nu_{1/2}$ ≤ 5000 Hz and ± 50 ppm when $\nu_{1/2} \geq 5000$ Hz. [b] N_3S_3 = 5-(4-amino-2-thiabutyl)-5-methyl-3,7-dithianonane-1,9-diamine; CLN_3S_3sar = 1-methyl-8-chloro-3,13,16-trithia-6,10,19-triazabicyclo-[6.6.6]icosane; $AMN_3S_3sarH^+$ = 1-methyl-8-ammonio-3,13,16-trithia-6,10,19-triazabicyclo[6.6.6]icosane; N_4S_2 = 5-(4-amino-2-azabutyl)-5-methyl-3,7-dithianonane-1,9-diamine; $AMN_4S_2sarH^+$ = 1-methyl-8-ammonio-3,13-dithia-6,10,16,19-tetraazabicyclo[6.6.6]icosane; daes = 3-thia-1,5-diaminopentane; N_5S = 5-methyl-5-(4-amino-2-thiabutyl)-3,7-diazanonane-1,9-diamine; $AZAN_5Ssar$ = 1-methyl-3-thia-6,8,10,13,16,19-hexaazabicyclo[6.6.6]icosane; HN_5Ssar = 1-methyl-3-thia-6,10,13,16,19-pentaazabicyclo[6.6.6]icosane; CLN_5Ssar = 1-methyl-8-chloro-3-thia-6,10,13,16,19-pentaazabicyclo[6.6.6]icosane; sep = 1,3,6,8,10,13,16,19-octaazabicyclo[6.6.6]icosane; $diAMN_6sarH_2^{2+}$ = 1,8-diammonio-3,6,10,13,16,19-hexaazabicyclo[6.6.6]icosane; $diNON_6sar$ = 1,8-dinitro-3,6,10,13,16,19-hexaazabicyclo[6.6.6]icosane; AMN_6sarH^+ = 1-methyl-8-ammonio-3,6,10,13,16,19-hexaazabicyclo[6.6.6]icosane; sen = 1,1,1-tris(4-amino-2-azabutyl)ethane. [c] used as primary reference. [d] $\nu_{1/2}$ is the separation of a ^{59}Co resonance at half its height.

^{59}Co NMR

The ^{59}Co chemical shifts were measured for the $[Co(RN_4S_2amp)]^{3+}$ (R = Pr, Bu, Xy) complexes as well as a series of hexadentate and encapsulating ligands with N_6, N_5S, N_4S_2, and N_3S_3 donor sets (data are reported in Table 7).

Both chemical shifts and line widths for ^{59}Co NMR have been found to be dependent on temperature, solvent, concentration and anion.[31] Thus ^{59}Co NMR studies of the amplector complexes employed 0.1 M solutions in H_2O at 301 K and deuterated solvents were not used to avoid the effects of deuterium exchange with amine groups, where applicable. The complexes $[Co(EtN_4S_2amp)]^{3+}$, $[Co(PrN_4S_2amp)]^{3+}$ and $[Co(BuN_4S_2amp)]^{3+}$ were studied as their mixed chloride/perchlorate salts. The $[Co(XyN_4S_2amp)]^{3+}$ complex was studied as its bromide salt. The ^{59}Co chemical shifts for $[Co(RN_4S_2amp)]^{3+}$ (R = Et, Pr, Bu and Xy: δ_{Co} 5638, 6125, 6223 and 6476 ppm, respectively) are similar although the line widths differ considerably ($\nu_{1/2}$ = 740, 1700, 2700 and 12000 Hz, respectively). The similarity of the ^{59}Co chemical shifts for these complexes is expected with the same coordination sphere about the cobalt nucleus for both complexes. The differences in line widths reflect the differences in electric field gradients at the cobalt nucleus caused by the departures of donor atoms from octahedral geometry as the size and rigidity of the R group increases.

Correlation between the ^{59}Co chemical shift and $E(^1A_{1g} \longrightarrow {}^1T_{1g})$

The series of cobalt(III) complexes of the mixed amine/thioether ligands and the amplector ligand offers an opportunity to further probe the relationship between the ^{59}Co magnetogyric ratio and the energy of $^1A_{1g} \longrightarrow {}^1T_{1g}$, the first ligand field transition.[9–11] This relationship has been tested previously, with varying degrees of success.[12–16]

The nonorthoaxial cobalt(III) complexes of the mixed amine/thioether and amplector ligands incorporate sigma donor ligands (primary and secondary amines) and π-acceptor donors (thioethers). The spectrophotometric and ^{59}Co NMR data (Tables 6 and 7) for a series of complexes were treated assuming nonorthoaxial geometry.[9–11] Use of the three ligand field parameters employed by Bramley (Δ, $B_{Schäffer}$ and D)[15,17] or the Racah B parameter determined from the ligand field analysis (eqn. 1) made little difference to the results obtained. Thus, the plot of the ^{59}Co magnetogyric ratio (γ_{Co}) *versus* $\beta(\Delta E)^{-1}$ for complexes with N_6, N_5S, N_4S_2 and N_3S_3 donors is shown in Fig. 4. Whilst most of the data points fall on a single line ($r^2 = 0.90$; $\gamma_0(^{59}Co) = 10.06 \pm 0.05$ MHz T^{-1} ○ data points) it is clear that data for the $[Co(RN_4S_2amp)]^{3+}$ (R = Pr, Bu and Xy) complexes (●, Fig. 4) do not correlate with the line of best fit for the other nitrogen–thioether complexes (○, Fig. 4).

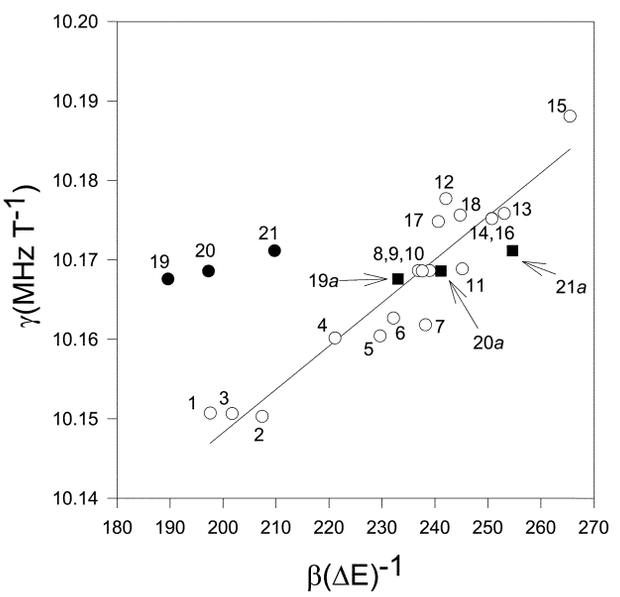

Fig. 4 Plot of ^{59}Co magnetogyric ratio *versus* $\beta(\Delta E)^{-1}$ for the series of complexes with N_6, N_5S, N_4S_2 and N_3S_3 donors (see Tables 6 and 7 for data).

Previously corrections to account for deviations from octahedral symmetry have been added in order to account for such variations from linearity.[12–16] In one case a correction term based on the angle of inclination (θ) of the metal–ligand bond with respect to the C_3 axis of the complex was employed.[16] Attempts to apply this correction to the $[Co(RN_4S_2amp)]^{3+}$ (R = Et, Pr, Bu and Xy) as well as the encapsulated complexes were not successful. Whilst an estimate of the position of the pseudo-C_3 axis was relatively straightforward for some complexes, for others the position of the pseudo-C_3 axis had to be adjusted to accommodate ligand bending. In addition, for the majority of complexes the average angle of inclination for Co–S bonds was distinctly different from that for the Co–N bonds. As a result it was necessary to consider θ as the average angle of inclination for all Co–S, Co–N bonds. Inclusion of this geometric parameter in the analysis resulted in a nonsystematic variation in calculated points and a poor correlation.

In order to more adequately explain the observed deviations from linearity of the γ_{Co} *versus* $\beta(\Delta E)^{-1}$ plot we sought to further investigate the bonding and spectroscopy of the Pr, Bu and

Table 8 Mulliken charge and covalency index for Co atoms, and HOMO–LUMO gap (in cm^{-1}) for $[CoRN_4S_2amp]^{3+}$ (R = Et, Pr, Bu, Xy) complexes. The $10D_q$ values calculated from spectroscopic data are given in parentheses

Complex	Co charge	Co covalency	HOMO–LUMO gap
$[Co(EtN_4S_2amp)]^{3+}$	+0.56	3.14	21859 (22570)
$[Co(PrN_4S_2amp)]^{3+}$	+0.61	3.02	21294 (21930)
$[Co(BuN_4S_2amp)]^{3+}$	+0.62	2.97	20891 (21780)
$[Co(XyN_4S_2amp)]^{3+}$	+0.51	3.31	13309

Xy complexes by means of density functional calculations on these species.

Bonding analysis

The results of the calculations on the $[Co(RN_4S_2amp)]^{3+}$ (R = Et, Pr, Bu, Xy) complexes investigated are summarized in Table 8, and Figs. 5 to 7. The results of bond valency calculations, including Mulliken charge and Mayer covalency for the Co atoms, and the energy gaps between the highest-occupied (HOMO) and lowest-unoccupied (LUMO) molecular orbitals for the four complexes investigated are given in Table 8.

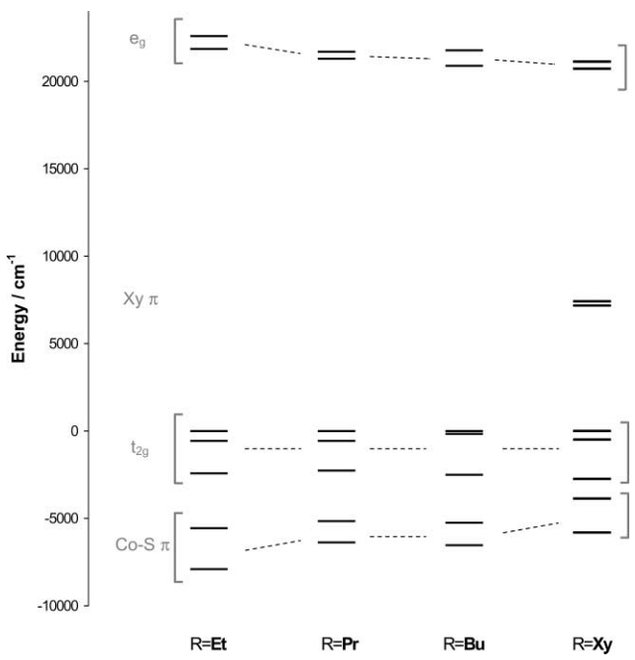

Fig. 5 Eigenvalue diagram showing some lowest-unoccupied and highest-occupied molecular orbital levels for $[Co(RN_4S_2amp)]^{3+}$ (R = Et, Pr, Bu, Xy).

The Mulliken charges and covalency indexes obtained suggest a slightly smaller degree of covalent character in the bonding to the Co site in the $[Co(PrN_4S_2amp)]^{3+}$ and $[Co(BuN_4S_2amp)]^{3+}$ complexes with respect to the $[Co(EtN_4S_2amp)]^{3+}$ system. This result disagrees with the observed trends in the Racah *B* parameters calculated from the spectroscopic data as the *B* values for $[Co(PrN_4S_2amp)]^{3+}$ and $[Co(BuN_4S_2amp)]^{3+}$ are at least 100 cm^{-1} lower than those for the $[Co(EtN_4S_2amp)]^{3+}$ complex. As discussed in the following section, this is probably a consequence of the particular nature of the electronic transitions in these complexes, which leads to unreliable results for the Racah *B* parameter when calculations are based on a (simple) d–d ligand-field model (eqn 1).

Eigenvalue diagrams for the $[Co(RN_4S_2amp)]^{3+}$ (R = Et, Pr, Bu, Xy) complexes are shown in Fig. 5. These diagrams include the lowest-unoccupied and highest-occupied energy levels that are most relevant to the discussion and interpretation of the electronic transitions presented in the next section. Although the actual molecular symmetry of all systems is C_1, it is possible to discuss the general properties of the molecular-orbital

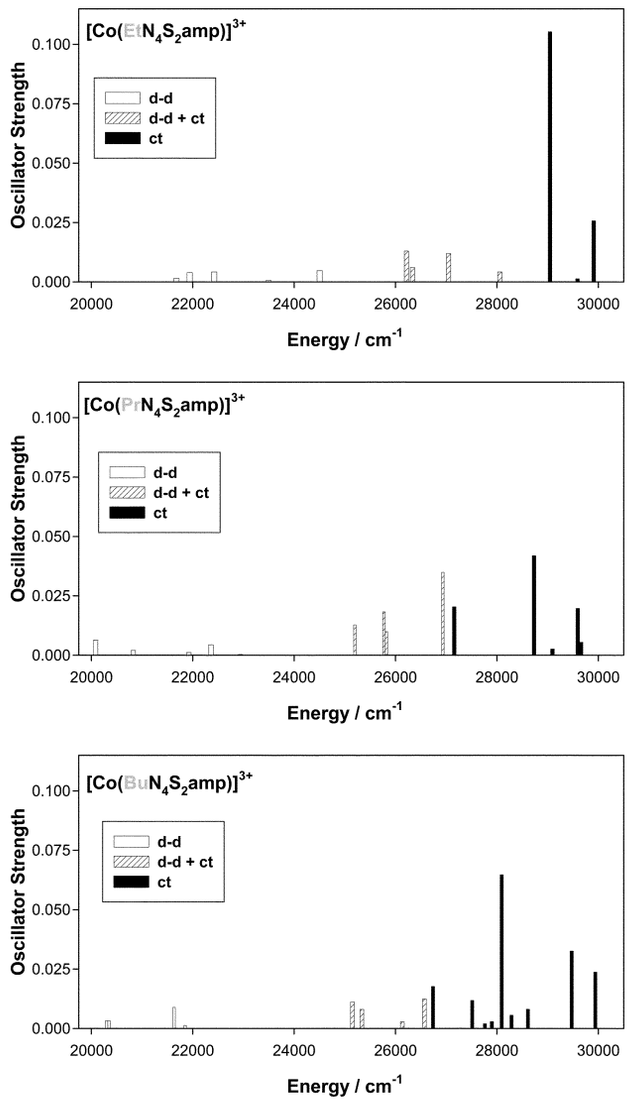

Fig. 6 Calculated electronic transitions for $[Co(RN_4S_2amp)]^{3+}$ (R = Et, Pr, Bu).

schemes by concentrating on the approximate octahedral environment of the $[CoN_4S_2]$ moiety.

For $[Co(RN_4S_2amp)]^{3+}$ (R = Et, Pr, Bu) the two lowest-unoccupied and the three-highest occupied orbitals can be associated, respectively, with the e_g and t_{2g} levels of a regular octahedral system. The splitting due to the low molecular symmetry is relatively small, amounting to 400–900 cm^{-1} for the e_g levels and 2200–2500 cm^{-1} for the t_{2g} levels, and the composition of these five orbitals is predominantly Co-d character. The two molecular orbitals lying below the t_{2g} levels involve significant contributions from both Co-d and S-p atomic orbitals, and generally exhibit Co–S bonding character. The HOMO–LUMO gaps for these three species mirror the trends in the $10D_q$ values obtained from spectroscopic measurements. A similar description can be applied to the $[CoXyN_4S_2amp]^{3+}$ complex, with the exception that two additional levels, lying between the e_g and t_{2g} orbitals, are observed. These levels correspond essentially to carbon-based π molecular orbitals associ-

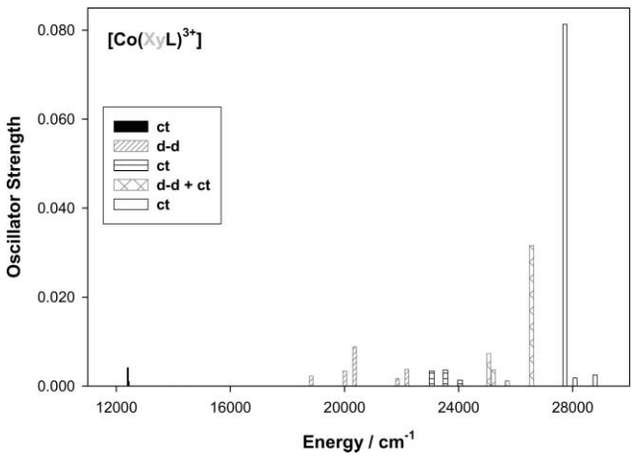

Fig. 7 Calculated electronic transitions for $[Co(XyN_4S_2amp)]^{3+}$.

ated with the Xy ring. The high-lying nature of these orbitals implies that the HOMO–LUMO gap in the $[Co(XyN_4S_2amp)]^{3+}$ complex is noticeably smaller that those in the $[Co(RN_4S_2amp)]^{3+}$ (R = Et, Pr, Bu) systems. However, the predicted separation of 20730 cm^{-1} between the e_g and t_{2g} levels is in good agreement with the observed $10D_q$ value of 21200 cm^{-1}.

Electronic excitations

The predicted energies and intensities of the singlet excitations, based on time-dependent density-functional calculations, are shown in Fig. 6 for $[Co(RN_4S_2amp)]^{3+}$ (R = Et, Pr, Bu) and in Fig. 7 for $[Co(XyN_4S_2amp)]^{3+}$. For all of these complexes, the low-symmetry splitting of the d–d and low-lying CT transitions gives rise to a number of allowed singlet excitations but a one-to-one mapping of the calculated bands with the split components of the $^1A_{1g} \longrightarrow {}^1T_{1g}$ and $^1A_{1g} \longrightarrow {}^1T_{2g}$ d–d transitions is not possible due to the mixing of d–d and CT transitions, particularly for the higher-lying $^1A_{1g} \longrightarrow {}^1T_{2g}$ transition. The general nature of the calculated electronic transitions is qualitatively consistent with the observed spectra for these complexes, particularly in relation to the lower energy shift of both the d–d and charge-transfer (CT) bands and also the mixing of d–d and CT transitions increasing in the order $[Co(RN_4S_2amp)]^{3+}$ (Et > Pr > Bu).

For $[Co(RN_4S_2amp)]^{3+}$ (R = Et, Pr, Bu) the calculated spin-allowed electronic transitions in the 20000–30000 cm^{-1} range are shown in Fig. 6, and these can be divided into three classes, corresponding to excitations with primarily d–d character, excitations with mixed d–d and CT character, and excitations with primarily CT character. All electronic transitions involve excitations to the e_g orbitals. The transitions exhibiting primarily d–d character occur at the lower end of the 20000–30000 cm^{-1} range, and are predominantly characterized by excitations involving electrons residing in the t_{2g} orbitals. The transitions occurring at the higher end of this range can be classified as ligand-to-metal CT, as these involve excitations from orbitals containing large ligand contributions (most commonly from S and C atoms). For the transitions predicted at energies intermediate between these two classes, both the d–d and CT components are important, the contributions from the Co-based t_{2g} orbitals and from the lower-lying orbitals (of greater ligand-based character) being similar. On the basis of Fig. 6, the spectra for the $[Co(PrN_4S_2amp)]^{3+}$ and $[Co(BuN_4S_2amp)]^{3+}$ complexes are predicted to be qualitatively similar, in particular, the mixed d–d/CT transitions have comparable or slightly lower intensities compared to the essentially pure CT transitions to higher energy. This is in contrast with the $[Co(EtN_4S_2amp)]^{3+}$ complex where the CT transitions have significantly higher intensities than the mixed d–d/CT transitions.

The trends observed in the comparison of the results for the $[Co(RN_4S_2amp)]^{3+}$ (R = Et, Pr, Bu) complexes indicate a shift of all three types of transitions to lower energy as the size of the R fragment increases. Also, the gap between the high-intensity CT and the d–d excitations is predicted to decrease and this is reflected in the relative intensities of the mixed d–d/CT and pure CT transitions discussed above. The smaller gap should lead to a greater degree of configuration interaction between the CT and d–d transitions in $[Co(PrN_4S_2amp)]^{3+}$ and $[Co(BuN_4S_2amp)]^{3+}$, and is probably the reason for the unusually small B values obtained for these complexes compared to $[Co(EtN_4S_2amp)]^{3+}$.

The Racah B parameter is calculated on the basis of a ligand-field model that assumes predominantly d–d character for all the experimental transitions used in the calculation. Therefore, if significant interaction between the d–d and CT excitations occurs (as is the case for $[Co(RN_4S_2amp)]^{3+}$ (R = Pr, Bu)) the application of this model is not strictly valid, and consequently the results obtained are not expected to be reliable. Theoretically, configuration interaction between the d–d and CT transitions will lower the energy of the $^1A_{1g} \longrightarrow {}^1T_{2g}$ d–d transition relative to $^1A_{1g} \longrightarrow {}^1T_{1g}$ and this in turn will result in a reduced B value as the energy gap between these two d–d transitions is given by 16B to first order.

The electronic transitions predicted by the time-dependent density functional calculations on $[Co(XyN_4S_2amp)]^{3+}$ (Fig. 7) include the three classes described for the $[Co(RN_4S_2amp)]^{3+}$ (R = Et, Pr, Bu) complexes, but two additional CT excitations can also be considered. These are represented by low-energy (11500–12500 cm^{-1}) excitations corresponding to transitions originating from the Xy-based orbitals lying between the e_g and t_{2g} levels (Fig. 5), and by relatively low-intensity ligand-to-metal CT excitations (occurring at 23000–24000 cm^{-1} and involving transitions from orbitals containing significant S and C contributions).

The calculations on $[Co(XyN_4S_2amp)]^{3+}$ predict a highly intense CT excitation (at approximately 28000 cm^{-1}), which lies close to the d–d transitions. This is consistent with the noted experimental difficulties in observing the $^1A_{1g} \longrightarrow {}^1T_{2g}$ transition due to the presence of an intense CT band.

The calculations suggest that the values of B for the $[Co(RN_4S_2amp)]^{3+}$ (R = Pr, 437 cm^{-1} Bu, 450 cm^{-1} Xy, 467 cm^{-1}), determined on the basis of a ligand-field model, are not accurate. On the basis of the previously determined B values, for example for the $[Co(EtN_4S_2amp)]^{3+}$ complex (551 cm^{-1}), it is reasonable to estimate that for the $[Co(RN_4S_2amp)]^{3+}$ (R = Pr, Bu, Xy) complexes B should be between 80–100 cm^{-1} larger than that determined. Reanalysis of the $\gamma(^{59}Co)$ *versus* $\beta_{Racah}(\Delta E)^{-1}$ data on this basis results in a more satisfactory fit to data for the three complexes in question (Fig. 4; assuming $B = B_{eqn\ (1)} + 100\ cm^{-1}$; ■ data points).

Conclusion

The synthetic procedure employed previously to prepare the $[Co(EtN_4S_2amp)]^{3+}$ complex has been extended to prepare a series of similar complexes $[Co(RN_4S_2amp)]^{3+}$ (R = Pr, Bu, Xy). The UV/visible spectra of the complexes are such that as the size of the R fragment increases, a lower energy shift of the three types of transitions (d–d, d–d/CT and CT) occurs with increasing mixing of d–d and CT transitions in the order $[Co(RN_4S_2amp)]^{3+}$ (Et > Pr > Bu). This mixing leads to an underestimation of the Racah B parameter when calculations are based on a (simple) d–d ligand-field model. In the present study, the underestimation for B becomes problematic as it significantly affects the correlation between γ_{Co} and $\beta(\Delta E)^{-1}$. For the series of nonorthoaxial N_6, N_5S, N_4S_2, N_3S_3 complexes investigated in this work the underestimation of B manifests itself clearly for the Pr, Bu and Xy complexes, the only complexes for which the orbital mixing (d–d, d–d/CT and CT) is significant. The result suggests that, in addition to the parameters employed previously in an attempt to reconcile the rel-

ationship between the magnetogyric ratio and $E(^1A_{1g} \longrightarrow {}^1T_{1g})$ the extent of orbital mixing should also be considered. It may be possible that a more reliable estimation of B can be obtained for Co(III) complexes using ^{59}Co NMR in conjunction with UV-visible spectroscopy compared with the use of UV-visible spectroscopy alone.

Experimental

Physical measurements

^{1}H, ^{13}C[^{1}H] and ^{13}C DEPT NMR spectra were recorded as described previously.[3] The chemical shifts of ^{13}C NMR spectra (D_2O) for the metal complexes are reported in parts per million (δ_C) as positive downfield and negative upfield of the internal reference 1,4-dioxane, as described previously.[3,4,7,8] For ^{13}C assignments, quaternary and aromatic carbons are denoted by C_q and Ar, respectively. ^{59}Co NMR spectra (0.1 M aqueous solutions) were recorded with a Bruker AV400 400 MHz NMR spectrometer in H_2O, without lock, at 301 K ($\nu_{1/2}$ = resonance line width (Hz) at half-height). Spectra were externally referenced to $[Co(en)_3]Cl_3$ in parts per million (δ_{Co}) at 7125 ppm. $K_3[Co(CN)_6]$ (0.1 M) was used as a secondary external reference at δ_{Co} 0 ppm.

Cyclic voltammetry and low resolution ESI mass spectrometry (ESI-MS) was performed as described previously.[3]

Solution and low temperature Nafion film UV-visible spectra were recorded as described previously.[3,4,7,8]

Calculation details

All density-functional calculations were carried out with the ADF (2002.03) program.[32–34] For geometry optimizations, functionals based on the Volko–Wilk–Nusair[35] (VWN) form of the Local Density Approximation[36] (LDA), and on the gradient-corrected expressions proposed by Perdew, Burke, and Ernzerhof[37] (PBE) were utilized. Calculations on all complexes investigated utilized C_1 molecular symmetry. Basis sets of triple-zeta quality and one (TZP) or two (TZ2P) polarization functions, incorporating frozen cores (Co.2p, C.1s, N.1s, S.2p), were employed.[32–34] Relativistic corrections were included using the ZORA appoach.[38–40] The population analysis, time-dependent density-functional-theory (TD-DFT) results and energy-level schemes were obtained by carrying out single-point calculations at the experimental geometry of the complexes. (The observed structural parameters of the Co–S–N–C framework were used but the positions of the H atoms were optimized). Atomic charges and valency indexes[41] were obtained (using an LDA/TZP computational scheme) with a program[42] designed for their calculation from the ADF output file. Calculations based on the TD-DFT approach employed the functional proposed by van Leeuwen and Baerends[43] (LB94) in conjuction with the PBE expressions, and the basis sets denoted TZ2P+ for Co and TZ2P for H, C, N, and S.[32–34]

Syntheses of ligands

1,3-(Dimethylmethylenedioxy)-2-methyl-2-hydroxymethylpropane, 1,3-(dimethylmethylenedioxy)-2-methyl-2-(methylene-*p*-tolylsulfonyl)propane and EtN_4S_2amp were prepared as described previously.[3] Xylenedithiol was prepared as described previously.[44]

2,10-bis(3,3-dimethyl-2,4-dioxocyclohexanyl)-4,8-dithiaundecane (1). To a solution of sodium metal (2.13 g, 93 mmol) dissolved in dry ethanol (150 cm^3) was added 1,3-propanedithiol (5.00 g, 46 mmol) and the solution stirred for five minutes. 1,3-(dimethylmethylenedioxy)-2-methyl-2-(methylene-*p*-toluenesulfonyl)propane (29.05 g, 92 mmol) was added and the solution heated at reflux for six hours. Upon cooling, the white precipitate of sodium tosylate was removed by filtration and the solvent was removed from the filtrate under reduced pressure. The residue was dissolved in $CHCl_3$ (300 cm^3) and the solution was washed with water (3 × 100 cm^3). The organic layer was separated, dried over Na_2SO_4, filtered and the solvent removed under reduced pressure leaving a yellow oil (16.0 g, 89%). ^{13}C NMR ($CDCl_3$): δ_C 19.3 (–CH_3); 20.7, 26.6 (CH_3–C_qO); 29.7 (–CH_2–); 32.7, 38.5 (–CH_2–S); 34.0 (C_q); 68.0 (–CH_2–O); 97.8 (C_q–O). ^{1}H NMR ($CDCl_3$): δ_H 0.87 (–CH_3, s); 1.40, 1.42 (CH_3–C_qO, s); 1.90 (–CH_2–, p); 2.66 (–CH_2(*hinge*)–S, t); 2.74 (–CH_2–S, s); 3.63 (–CH_2–O, dd).

2,2,10,10-tetra(hydroxymethyl)-4,8-dithiaundecane (2). 1 (20.0 g) was dissolved in ethanol (400 cm^3) and heated at reflux. Concentrated HCl (20 cm^3) was added and the reflux continued for ten minutes. Upon cooling the solvent was removed under reduced pressure to give a brown oil (16.8 g, quantitative). ^{13}C NMR (d_4-methanol): δ_C 18.9 (–CH_3); 30.8 (–CH_2–); 33.5, 38.4 (–CH_2–S); 42.2 (C_q); 67.2 (–CH_2–O). ^{1}H NMR (d_4-methanol): δ_H 0.90 (–CH_3, s); 1.84 (–CH_2–,p); 2.57 (–CH_2–S, s); 2.63 (–CH_2(*hinge*)–S, t); 3.46 (–CH_2–O, s).

2,2,10,10-tetra(methylene-*p*-toluenesulfonyl)-4,8-dithiaundecane (3). 2 (14.4 g) was dissolved in dry pyridine (200 cm^3) and cooled in an ice bath. To this stirred solution, *p*-toluenesulfonyl chloride (38.5 g) in dry pyridine (250 cm^3) was added drop wise over two hours. The reaction mixture was allowed to warm to room temperature and stirring maintained for 48 hours. The mixture was poured into a solution of concentrated HCl (275 cm^3), water (350 cm^3) and methanol (700 cm^3), which precipitated an off-white solid that was extracted in $CHCl_3$ (3 × 300 cm^3). The extracts were combined and washed with water (2 × 300 cm^3). The $CHCl_3$ solution was separated, dried over Na_2SO_4, filtered and the solvent was removed under reduced pressure leaving a yellow oil (45.5 g, quantitative). ^{13}C NMR ($CDCl_3$): δ_C 18.2 (–CH_3); 21.7 (–CH_3(tosylate)); 29.2 (–CH_2–); 32.5, 36.4 (–CH_2–S); 39.6 (C_q); 71.6 (–CH_2–O); 127.8, 129.9, 132.1, 145.1 (Ar(tosylate)). ^{1}H NMR ($CDCl_3$): δ_H 0.92 (–CH_3, s); 2.45 (–CH_3(tosylate), –CH_2–S, s); 3.83 (–CH_2–O, dd); 7.54 (Ar–H(tosylate), dd).

2,2,10,10-tetra(methylenephthalimido)-4,8-dithiaundecane (4). 3 (41.35 g) and potassium phthalimide (36.3 g) were suspended in diethylene glycol dimethyl ether (100 cm^3) and the mixture heated at 150 °C for 18 hours. The cooled solution was poured into water (600 cm^3) to precipitate a brown oil. The solution was decanted and the remaining brown oil dissolved in $CHCl_3$ (600 cm^3), dried over Na_2SO_4, filtered and the solvent removed under reduced pressure to give a pale brown oil (38.9 g). The product was used without further purification.

2,2,10,10-tetra(methyleneamine)-4,8-dithiaundecane (PrN_4S_2-amp) (5). 4 (22.3 g) was suspended in ethanol (300 cm^3) and heated at reflux. Hydrazine hydrate (42 cm^3) was added to the refluxing solution. Over a period of five minutes the solution became clear then a dense white precipitate formed. The reflux was maintained for two hours. The solution was cooled in an ice bath and concentrated HCl (40 cm^3) was added dropwise. The mixture was heated at reflux for a further 40 minutes, then cooled and the solvent removed under reduced pressure. The residue was dissolved in water (200 cm^3) and the solution filtered. The filtrate was made strongly alkaline with KOH and the product was extracted in $CHCl_3$ (3 × 100 cm^3). The $CHCl_3$ extracts were combined, dried over Na_2SO_4, filtered and the solvent was removed under reduced pressure to yield a yellow oil (4.22 g). The product was used for preparation of the cobalt(III) complex without further purification.

2,11-bis(3,3-dimethyl-2,4-dioxocyclohexanyl)-4,9-dithiadodecane (6). Prepared as described for **1** using sodium metal (1.90 g, 83 mmol) dissolved in dry ethanol (150 cm^3), 1,4-butanedithiol (5.00 g, 41 mmol) and 1,3-(dimethylmethyl-

ene dioxy)-2-methyl-2-(methylene-*p*-toluenesulfonyl)propane (25.70 g, 0.082 mol). A golden oil resulted (16.0 g, 96%). ^{13}C NMR ($CDCl_3$): δ_C 19.2 (–CH_3); 20.6, 26.6 (*C*H_3–C_qO); 28.6 (–CH_2–); 33.5, 38.4 (–CH_2–S); 34.0 (C_q); 67.9 (–CH_2–O); 97.7 (C_q–O). ^{1}H NMR ($CDCl_3$): δ_H 0.86 (–CH_3, s); 1.39, 1.41 (CH_3–C_qO, s); 1.71 (–CH_2–, m); 2.56 (–CH_2(*hinge*)–S, t); 2.72 (–CH_2–S, s); 3.63 (–CH_2–O, dd).

2,2,11,11-tetra(hydroxymethyl)-4,9-dithiadodecane (7). Prepared as described for **2** using **6** (16.0 g) to yield a white–grey residue on standing (16.8 g, quantitative). ^{13}C NMR (d_4-methanol): δ_C 18.9 (–CH_3); 29.8 (–CH_2–); 34.4, 38.4 (–CH_2–S); 42.2 (C_q); 67.2 (–CH_2–O). ^{1}H NMR (d_4-methanol): δ_H 0.90 (–CH_3, s); 1.68 (–CH_2–, m); 2.57 (–CH_2–S, s +m); 3.45 (–CH_2–O, s).

2,2,11,11-tetra(methylene-*p*-toluenesulfonyl)-4,9-dithiadodecane (8). Prepared as described for **3** using **7** (15.0 g), *p*-toluenesulfonyl chloride (38.5 g) in dry pyridine (250 cm^3). A golden oil was obtained (37.0 g, 85%). ^{13}C NMR ($CDCl_3$): δ_C 18.1 (–CH_3); 21.5 (–CH_3(tosylate)); 28.3 (–CH_2–); 33.5, 36.4 (–CH_2–S); 39.6 (C_q); 71.6 (–CH_2–O); 127.8, 129.9, 132.0, 145.0 (Ar(tosylate)). ^{1}H NMR ($CDCl_3$): δ_H 0.92 (–CH_3, s); 1.53 (–CH_2–, m); 2.40 (–CH_2 (*hinge*)–S, m); 2.45 (–CH_3(tosylate), –CH_2–S, s); 3.83 (–CH_2–O, dd); 7.55 (Ar–H(tosylate), dd).

2,2,11,11-tetra(methylenephthalimido)-4,9-dithiadodecane (9). Prepared as described for **4** using **8** (14.9 g), potassium phthalimide (12.9 g) in diethylene glycol dimethyl ether (100 cm^3) to yield a brown solid (18.0 g). The product was used without further purification.

2,2,11,11-tetra(methyleneamine)-4,9-dithiadodecane (BuN_4S_2-amp) (10). Prepared as described for **5** using **9** (18.0 g) in ethanol (250 cm^3) and hydrazine hydrate (45 cm^3) to yield a golden oil (4.6 g). The product was used for preparation of the cobalt(III) complex without further purification.

1,2-bis(4-(3,3-dimethyl-2,4-dioxocyclohexanyl)-2-thiapentyl)-benzene (11). Prepared as described for **1** using sodium metal (1.59 g, 69 mmol) dissolved in dry ethanol (250 cm^3), xylenedithiol (5.9 g, 35 mmol) and 1,3-(dimethylmethylenedioxy)-2-methyl-2-(methylene-*p*-toluenesulfonyl)propane (21.8 g, 69 mmol). A yellow oil resulted (17.7 g, quantitative). ^{13}C NMR ($CDCl_3$): δ_C 19.4 (–CH_3); 20.9, 26.5 (*C*H_3–C_qO); 34.1 (C_q); 35.4, 38.2 (–CH_2–S); 68.1 (–CH_2–O); 98.0 (C_q–O); 127.2 (Ar–); 130.6, 136.5 (Ar–H). ^{1}H NMR ($CDCl_3$): δ_H 0.86 (–CH_3, s); 1.39, 1.41 (CH_3–C_qO, s); 2.71 (–CH_2–S, s); 3.62 (–CH_2–O, dd); 3.93 (–CH_2–Ar, s); 7.21 (Ar–H, m).

1,2-bis(4,4-di(methylenehydroxy)-2-thiapentyl)benzene (12). Prepared as described for **2** using **11** (17.0 g) to yield a yellow oil (14.1 g, quantitative) which was immediately used. ^{13}C NMR (d_4-methanol): δ_C 19.0 (–CH_3); 36.2, 38.3 (–CH_2–S); 42.3 (C_q); 67.2 (–CH_2–O); 128.2, 131.7 (Ar–H); 138.1 (Ar–). ^{1}H NMR (d_4-methanol): δ_H 0.89 (–CH_3, s); 2.58 (–CH_2–S, s); 3.45 (–CH_2–O, s); 3.93 (–CH_2–Ar, s); 7.21 (Ar–H, m).

1,2-bis(4,4-di(methylene-*p*-toluenesulfonyl)-2-thiapentyl)-benzene (13). Prepared as described for **3** using **12** (14.1 g) and *p*-toluenesulfonyl chloride (31.4 g) in dry pyridine (250 cm^3). The initial product was treated with activated charcoal to yield a golden oil (21.0 g, 56%). ^{13}C NMR ($CDCl_3$): δ_C 18.1 (–CH_3); 21.5 (–CH_3(tosylate)); 35.1, 35.9 (–CH_2–S); 71.5 (–CH_2–O); 127.6, 130.0 (Ar–H); 127.8, 129.9, 132.0, 145.1 (Ar(tosylate)); 135.6 (Ar–). ^{1}H NMR ($CDCl_3$): δ_H 0.88 (–CH_3, s); 2.44 (–CH_3(tosylate), –CH_2–S, s); 3.78 (–CH_2–O, –CH_2–Ar, m); 7.16 (Ar–H, m); 7.53 (Ar–H(tosylate), dd).

1,2-bis(4,4-di(methylenephthalimido)-2-thiapentyl)benzene (14). Prepared as described for **5** using **13** (32.0 g) and potassium phthalimide (26.1 g) in diethylene glycol dimethyl ether (150 cm^3) to yield a brown oil (42.3 g). The product was isolated and used without further purification.

1,2-bis(4,4-methyleneamine)-2-thiapentyl)benzene (XyN_4S_2-amp) (15). Prepared as described for **5** using **14** (20.9 g) in ethanol (250 cm^3) and hydrazine hydrate (48 cm^3) to yield a golden oil (6.7 g). The product was used for preparation of the cobalt(III) complex without further purification.

Synthesis of metal complexes

Caution. Although the perchlorate salts described in this work do not appear to be sensitive to shock or heat, these materials, like all perchlorates, should be treated with caution.

[Co(PrN_4S_2amp)]Cl(ClO_4)$_2$·2H_2O. The complex was prepared using cobaltous nitrate hexahydrate (13.9 g) in methanol (250 cm^3) added dropwise to the stirred crude ligand mixture (13.9 g) dissolved in methanol (200 cm^3) following the procedure reported for the analogous EtN_4S_2amp complex. The orange-red solid (0.7 g, 3.3%) resulting after chromatographic purification was crystallized from water with sodium perchlorate to give red crystals. Analysis. Calculated for [$C_{13}H_{32}N_4S_2$Co]Cl(ClO_4)$_2$·2H_2O: C, 24.48; H, 5.69; N, 8.79%. Found: C, 23.71; H, 5.42; N, 8.49%. UV-visible spectrum [λ_{max}/nm (ε_{max}/L mol^{-1} cm^{-1}) in H_2O]: 489 (300), 374 (250), 294 (19600). ^{13}C NMR (D_2O): δ_C −44.8 (–CH_2–); −43.1 (–CH_3); −32.3, −29.0 (–CH_2–S); −26.3 (C_q); −21.7, −21.3 (–CH_2–N). ^{1}H NMR (D_2O): δ_H 1.04 (–CH_3, s); 2.2–3.2 (CH_2, m). ^{59}Co NMR (H_2O): δ_{Co} 6125 ($\nu_{1/2}$ = 1700 Hz). ESI-MS: Calculated for [Co(PrN_4S_2amp)]$^{3+}$ − 2H^+: *m*/*z* 365; found: *m*/*z* 365 (88%).

[Co(BuN_4S_2amp)]Cl$_2$(ClO_4)·2H_2O. The complex was prepared using cobaltous nitrate hexahydrate (4.6 g) in methanol (250 cm^3) added dropwise to the stirred crude ligand mixture (4.6 g) dissolved in methanol (200 cm^3) following the procedure reported for the analogous EtN_4S_2amp complex. After chromatographic purification a red solid (0.90 g, 13%) was obtained. The solid was dissolved in water and $NaClO_4$ added and the solution was left to stand overnight to give large red crystals. Analysis. Calculated for [$C_{14}H_{34}N_4S_2$Co]Cl$_2$(ClO_4)·2H_2O: C, 28.60; H, 6.52; N, 9.53%. Found: C, 28.03; H, 6.69; N, 9.43%. UV-visible spectrum [λ_{max}/nm (ε_{max}/L mol^{-1} cm^{-1}) in H_2O]: 496 (348), 296 (10400), 236 (8250). ^{13}C NMR (D_2O): δ_C −43.1 (–CH_3); −37.7 (–CH_2-(*hinge*)); −26.5 (C_q); −22.4 (–CH_2–S); −22.0, −21.7 (–CH_2–N); −21.0 (–CH_2(*hinge*)–S). ^{1}H NMR (D_2O): δ_H 1.09 (–CH_3, s); 1.9–3.3 (CH_2, m). ^{59}Co NMR (H_2O): δ_{Co} 6223 ($\nu_{1/2}$ = 2700 Hz). ESI-MS: Calculated for [Co(BuN_4S_2amp)]$^{3+}$ − H^+ + $^{35}ClO_4^-$: *m*/*z* 479; found: *m*/*z* 479 (100%). Calculated for [Co(BuN_4S_2amp)]$^{3+}$ − 2H^+: *m*/*z* 379; found: *m*/*z* 379 (40%).

[Co(XyN_4S_2amp)]Br$_3$·3H_2O. The complex was prepared as described above from cobaltous nitrate hexahydrate (13.5 g) in methanol (250 cm^3) and the crude ligand mixture (13.5 g) dissolved in methanol (200 cm^3). After chromatographic purification a red–pink solid (0.3 g, 1.5%) was obtained. The solid was crystallized from aqueous solution with KBr to give red crystals. Analysis. Calculated for [$C_{18}H_{34}N_4S_2$Co]Br$_3$·3H_2O requires C, 29.89; H, 5.57; N, 7.75%. Found: C, 29.71; H, 5.29; N, 7.59%. UV-visible spectrum [λ_{max}/nm (ε_{max}/L mol^{-1} cm^{-1}) in H_2O]: 506 (260), 303 (11800). ^{13}C NMR (D_2O): δ_C −43.0 (–CH_3); −30.3, −29.0 (–CH_2–S); −28.7 (C_q); −21.9, −21.6 (–CH_2–N); 63.9 (Ar–); 64.1, 66.1 (Ar–H). ^{1}H NMR (D_2O): δ_H 1.07 (–CH_3, s); 2.1–4.6 (CH_2, m); 7.56 (Ar–H, s). ^{59}Co NMR (H_2O): δ_{Co} 6476 ($\nu_{1/2}$ = 12000 Hz). ESI-MS: Calculated for [Co(XyN_4S_2amp)]$^{3+}$ − H^+ + $^{80}Br^-$: *m*/*z* 508; found: *m*/*z* 508

(18%). Calculated for $[Co(XyN_4S_2amp)]^{3+} - 2H^+$: *m*/*z* 427; found: *m*/*z* 427 (9%).

Crystal structure determinations

For diffractometry the crystals were mounted onto glass fibres with Supa Glue. Lattice parameters were determined by least squares fits to the setting parameters of 25 independent reflections, measured and refined with an Enraf-Nonius CAD4 diffractometer using graphite-monochromated Mo Kα radiation. The structures were solved by heavy-atom methods (direct methods) and refined using full-matrix least squares on F^2. Hydrogen atoms from the organic ligands were fixed in idealised positions while those from non-coordinated water molecules were not found and were unable to be refined. Programs used were SHELXS-86,[45] and SHELXL-97[46] for solution and refinement, respectively, and ORTEP[47] for plotting. Crystal data are given in Table 1. The geometries of the molecules are shown in Fig. 1, 2 and 3 together with atomic numbering schemes. Selected bond lengths and bond angles are given in Tables 2, 3 and 4.

CCDC reference numbers 222245–222247.

See http://www.rsc.org/suppdata/dt/b3/b313189k/ for crystallographic data in CIF or other electronic format.

References

1 F. Lions, *Rec. Chem. Prog.*, 1961, **22**, 69.
2 A. T. Baker, *J. Proc. R. Soc. N.S.W.*, 1999, **132**, 65.
3 C. A. Sharrad, S. R. Lüthi and L. R. Gahan, *Dalton Trans.*, 2003, 3693.
4 T. M. Donlevy, L. R. Gahan, T. W. Hambley, K. L. McMahon and R. Stranger, *Aust. J. Chem.*, 1993, **46**, 1799.
5 L. R. Gahan, T. W. Hambley, A. M. Sargeson and M. R. Snow, *Inorg. Chem.*, 1982, **21**, 2699.
6 L. R. Gahan, T. M. Donlevy and T. W. Hambley, *Inorg. Chem.*, 1990, **29**, 1451.
7 T. M. Donlevy, L. R. Gahan, T. W. Hambley and R. Stranger, *Inorg. Chem.*, 1992, **31**, 4376.
8 J. I. Bruce, L. R. Gahan, T. W. Hambley and R. Stranger, *Inorg. Chem.*, 1993, **32**, 5997.
9 R. Freeman, G. R. Murray and R. E. Richards, *Proc. R. Soc. London, Ser. A*, 1957, **242**, 455.
10 N. F. Ramsay, *Phys. Rev.*, 1950, **77**, 567.
11 J. S. Griffith and L. E. Orgel, *Trans. Faraday Soc.*, 1957, **53**, 601.
12 N. Juranić, M. B. Ćelap, D. Vučelić, M. J. Malinar and P. N. Radivojša, *J. Magn. Reson.*, 1979, **35A**, 319.
13 N. Juranić, *Inorg. Chem.*, 1983, **22**, 521.
14 N. Juranić, *Inorg. Chem.*, 1980, **19**, 1093.
15 R. Bramley, M. Brorson, A. M. Sargeson and C. E. Schäffer, *J. Am. Chem. Soc.*, 1985, **107**, 2780.
16 N. Juranić, *J. Serb. Chem. Soc.*, 1991, **56**, 723.
17 C. E. Schäffer, *Proc. R. Soc. London, Ser. A*, 1967, **A297**, 96 (note the subscript for $B_{Schäffer}$ is used as a distinction between this low-symmetry parameter and Racah parameter *B*).
18 G. A. Bottomley, I. J. Clark, I. I. Creaser, L. M. Engelhardt, R. J. Geue, K. S. Hagan, J. M. Harrowfield, G. A. Lawrance, P. A. Lay, A. M. Sargeson, A. J. See, B. W. Skelton, A. H. White and F. R. Wilner, *Aust. J. Chem.*, 1994, **47**, 143.
19 A. M. Sargeson, *Pure Appl. Chem.*, 1986, **58**, 1511.
20 I. J. Clark, R. J. Geue, L. M. Engelhardt, J. M. Harrowfield, A. M. Sargeson and A. H. White, *Aust. J. Chem.*, 1993, **46**, 1485.
21 I. I. Creaser, J. M. Harrowfield, A. J. Herlt, A. M. Sargeson, J. Springborg, R. J. Geue and M. R. Snow, *J. Am. Chem. Soc.*, 1977, **99**, 3181.
22 *lel* and *ob* refer to limiting conformations of five membered chelate rings in which the C–C axis is respectively parallel and oblique to the pseudo-C_3 axis of the complex cation. See *Inorg. Chem.*, 1970, **9**, 1. For six and seven membered chelate rings the same designation is applied to the vector between carbon atoms immediately bonded to ligand donor atoms, as opposed to a C–C axis.
23 P. Hendry and A. Ludi, *Adv. Inorg. Chem.*, 1990, **35**, 117.
24 P. Osvath, A. M. Sargeson, A. McAuley, R. E. Mendelez, S. Subramanian, M. J. Zaworotko and L. Broge, *Inorg. Chem.*, 1999, **38**, 3634.
25 G. J. Grant, S. S. Shoup, C. L. Baucom and W. N. Setzer, *Inorg. Chim. Acta*, 2001, **317**, 91.
26 G. Wei, C. C. Allen, T. W. Hambley, G. A. Lawrance and M. Maeder, *Inorg. Chim. Acta*, 1997, **261**, 197.
27 R. J. Geue and M. R. Snow, *Inorg. Chem.*, 1977, **16**, 231.
28 R. A. D. Wentworth and T. S. Piper, *Inorg. Chem.*, 1965, **4**, 709.
29 A. B. P. Lever, *Inorganic Electronic Spectroscopy*, 2nd edn., Elsevier Publ., Amsterdam, 1984.
30 C. R. Hare, in *Spectroscopy and Structure of Metal Chelate Compounds*, ed. K. Nakamoto and P. J. McCarthy, John Wiley & Sons, New York, 1968.
31 R. G. Kidd and R. J. Goodfellow, in *NMR and the Periodic Table*, ed. R. K. Harris and B. E. Mann, Academic Press, London, 1978.
32 *ADF2002.03*, SCM, Theoretical Chemistry, Vrije Universiteit, Amsterdam, The Netherlands, http://www.scm.com.
33 C. Fonseca Guerra, J. G. Snijders, G. te Velde and E. J. Baerends, *Theor. Chem. Acc.*, 1998, **99**, 391.
34 G. te Velde, F. M. Bickelhaupt, S. J. A. van Gisbergen, C. Fonseca Guerra, E. J. Baerends, J. G. Snijders and T. Ziegler, *J. Comput. Chem.*, 2001, **22**, 931.
35 S. H. Vosko, L. Wilk and M. Nusair, *Can. J. Phys.*, 1980, **58**, 1200.
36 W. Kohn and L. J. Sham, *Phys. Rev.*, 1965, **140**, A1133.
37 J. P. Perdew, K. Burke and M. Ernzerhof, *Phys. Rev. Lett.*, 1996, **77**, 3865.
38 E. van Lenthe, E. J. Baerends and J. G. Snijders, *J. Chem. Phys.*, 1993, **99**, 4597.
39 E. van Lenthe, E. J. Baerends and J. G. Snijders, *J. Chem. Phys.*, 1994, **101**, 9783.
40 E. van Lenthe, A. E. Ehlers and E. J. Baerends, *J. Chem. Phys.*, 1999, **110**, 8943.
41 I. Mayer, *Chem. Phys. Lett.*, 1983, **97**, 270.
42 A. J. Bridgeman and C. J. Empson, MAYER, University of Hull, United Kingdom, 2002.
43 R. van Leeuwen and E. J. Baerends, *Phys. Rev. A*, 1994, **49**, 2421.
44 T. Takata, M. Kanamaru and T. Endo, *Macromolecules*, 1997, **30**, 6721.
45 G. M. Sheldrick, SHELXS-86, in Crystallographic Computing 3, ed. G. M. Sheldrick, C. Kruger and R. Goddard, Oxford University Press, Oxford, UK, 1985, pp. 175–189.
46 G. M. Sheldrick, SHELXL-97, Program for refinement of crystal structures, University of Göttingen, Germany, 1997, Release 97–2.
47 C. K. Johnson, ORTEP, A Thermal Ellipsoid Plotting Program, Oak Ridge National Laboratory, Oak Ridge, TN, 1965.
48 *PeakFit*, AISN Software Inc., 1991–1995, version 4.
49 L. R. Gahan, T. W. Hambley, G. H. Searle, M. J. Bjerrum and E. Larsen, *Inorg. Chim. Acta*, 1988, **147**, 17.
50 C. K. Jørgensen, *Absorption Spectra and Chemical Bonding in Complexes*, Pergamon Press: London, 1962.
51 I. Creaser, R. J. Geue, J. MacB. Harrowfield, A. J. Herlt, A. M. Sargeson, M. R. Snow and J. Springborg, *J. Am. Chem. Soc.*, 1982, **104**, 6016.
52 R. J. Geue and G. H. Searle, *Aust. J. Chem.*, 1983, **36**, 927.